Dynamic Response of 6MW Spar Type Floating Offshore Wind Turbine by Experiment and Numerical Analyses

China Ocean Eng., 2020, Vol. 34, No. 5, P. 608–620
DOI: https://doi.org/10.1007/s13344-020-0055-z, ISSN 0890-5487
http://www.chinaoceanengin.cn/ E-mail: coe@nhri.cn

Dynamic Response of 6MW Spar Type Floating Offshore Wind Turbine by Experiment and Numerical Analyses

MENG Long[a, b, c, d], HE Yan-ping[a, b, c, *], ZHAO Yong-sheng[a, b, c, *], YANG Jie[a, b, c], YANG He[e], HAN Zhao-long[a, c], YU Long[a, b, c], MAO Wen-gang[f], DU Wei-kang[g]

[a] State Key Laboratory of Ocean Engineering, Shanghai Jiao Tong University, Shanghai 200240, China

[b] Collaborative Innovation Center for Advanced Ship and Deep-Sea Exploration (CISSE), Shanghai Jiao Tong University, Shanghai 200240, China

[c] School of Naval Architecture, Ocean & Civil Engineering, Shanghai Jiao Tong University, Shanghai 200240, China

[d] China Aerodynamics Research and Development Center, Mianyang, 621000, China

[e] Ocean Engineering Department, Texas A&M University, College Station, TX 77843, USA

[f] Department of mechanics and Maritime Sciences, Chalmers University of Technology, 41296, Gothenburg, Sweden

[g] Ocean Engineering Group, Department of Civil, Architecture and Environmental Engineering, University of Texas at Austin, Texas, TX 78712, USA

Received October 26, 2019; revised April 23, 2020; accepted May 24, 2020

Abstract

The floating offshore wind turbine (FOWT) is widely used for harvesting marine wind energy. Its dynamic responses under offshore wind and wave environment provide essential reference for the design and installation. In this study, the dynamic responses of a 6MW Spar type FOWT designed for the water depth of 100 m are investigated by means of the wave tank experiment and numerical analysis. A scaled model is manufactured for the experiment at a ratio of 65.3, while the numerical model is constructed on the open-source platform FAST (Fatigue, Aerodynamics, Structures, and Turbulence). Still water tests, wind-induced only tests, wave-induced only tests and combined wind-wave-current tests are all conducted experimentally and numerically. The accuracy of the experimental set-up as well as the loading generation has been verified. Surge, pitch and heave motions are selected to analyze and the numerical results agree well with the experimental values. Even though results obtained by using the FOWT calculation model established in FAST software show some deviations from the test results, the trends are always consistent. Both experimental and numerical studies demonstrate that they are reliable for the designed 6MW Spar type FOWT.

Key words: floating offshore wind turbine, dynamic responses, Spar type platform, FAST, model test

Citation: Meng, L., He, Y. P., Zhao, Y. S., Yang, J., Yang, H., Han, Z. L., Yu, L., Mao, W. G., Du, W. K., 2020. Dynamic response of 6mw spar type floating offshore wind turbine by experiment and numerical analyses. China Ocean Eng., 34(5): 608–620, doi: https://doi.org/10.1007/s13344-020-0055-z

1 Introduction

In recent decades, energy consumption has enormously increased worldwide. In accordance with the Kyoto Protocol, the goal of producing 22.1% of energy from renewable sources by the year of 2020 has been set by the European Union (Tomasicchio et al., 2018). Such renewable sources include the energy of wave, wind, tidal power, etc. (Iuppa et al., 2015; Contestabile et al., 2015; Uihlein and Magagna, 2016; Soukissian et al., 2017), among which the wind energy could be one of the most prominent renewable energy sources (Sahu, 2018; Global Wind Statistics, 2016). Compared with the onshore wind resources, the offshore wind energy increasingly attracts researchers' interest due to its high energy density and low turbulence (Marino et al., 2017; Tran and Kim, 2015). At present, the exploitation of offshore wind energy has been a trend of edge-cutting for wind energy industry. Thus, offshore wind turbines play an important role to efficiently convert wind energy resources into electricity.

To take the advantage of the stronger and steadier offshore wind (Wen et al., 2018), in recent years, deploying the FOWT in deep ocean has been widely discussed. Several

Foundation item: This research was financially supported by the National Natural Science Foundation of China (Grant Nos. 51809170 and 51879160), the National Key R&D Program of China (Grant No. 2019YFB1503700), Program for Intergovernmental International S&T Cooperation Projects of Shanghai Municipality (Grant Nos.19160713600 and 18160744000), and the Program for Professor of Special Appointment (Eastern Scholar) at Shanghai Institutions of Higher Learning (Grant Nos. ZXDF010037 and ZXDF010040).

*Corresponding authors. E-mail: hyp110@sjtu.edu.cn; yongsheng@sjtu.edu.cn

types of FOWT (as shown in Fig.1) in deep water, such as Spar type, TLP (Tension Leg Platform) type, barge type and semi-submersible type have been proposed and investigated (Matha, 2010; Jonkman, 2010; Karimirad and Moan, 2012a). They take the advantages of these typical offshore platform types to provide sufficient stability for offshore wind turbine operation. In addition, the multiple-point mooring system is widely adopted for these FOWTs, except for the TLP type which is moored by vertical taut lines.

Compared with other types of FOWT, the Spar type FOWT is a promising option because of its simple structure and good stability. The Spar type platform is a long cylinder, which largely immerges into the water and thus provides enough buoyancy. A catenary spread mooring system using anchor-chains, steel cables and/or synthetic fiber ropes could add on dynamic stability. It is of great significance to investigate the difference brought about by the installation of wind turbine atop the floating Spar platform.

The research of Spar type FOWT is multidisciplinary, involving aerodynamics, hydrodynamics, multi-structure dynamics (elastic) and automatic control (Namik and Stol, 2010; Wang and Sweetman, 2013; Jeon et al., 2014; Salehyar and Zhu, 2015; Nejad et al., 2015). The research on numerical calculation methods of Spar type FOWT is concentrated in the United States, Norway and the Netherlands. For the study of aerodynamic performance of Spar type FOWT, many researchers generally use Blade Element Momentum (BEM) theory, Generalized Dynamic Wake (GDW) theory and Computational Fluid Dynamics (CFD) method (Chaviaropoulos and Hansen, 2000). Based on the linear wave theory, Morrison equation is commonly used in the study of hydrodynamic performance of Spar type FOWT (Utsunomiya et al., 2009). In order to analyze the fully coupled analysis of Spar type FOWT, several simulation tools have been developed and released in the OC3 and OC4 projects (Karimirad, 2011; Kvittema et al., 2012; Quallen et al., 2013). Among those numerical research softwares, FAST platform is widely used due to its aerodynamic-hydrodynamic-elastic-servo full coupled analysis function and fast calculation. But, owing to the complexity of these models, their accuracy and reliability ask for more validation with measured data from the site or model tests. Compared with the field data, the model testing results are more accessible to verify various concepts and mathematical models.

However, for offshore wind turbine model tests, some modifications are always adopted because of the difficulty in satisfying the hydrodynamic and aerodynamic similarity simultaneously. UC Berkeley conducted a model test on the WindFloat FOWT concept with a scale ratio of 1:67. The Froude number was uniform between the model and the prototype, whereas the aerodynamic similarity was not met. Thus, a disk was applied to simulate the wind rotor (Cermelli et al., 2009). Another 1:47 Froude scaled model test of the Hywind Spar type FOWT was conducted under a variety of sea states at Ocean Basin Laboratory at Marintek (Nielsen et al., 2006; Skaare et al., 2007; Skaare, 2017). During this test, the rotor was driven by the motor at the rear of the nacelle to control its speed. Moreover, a 1:50 scale model of OC3 Spar type FOWT was made at the State Key Laboratory of Ocean Engineering at Shanghai Jiao Tong University (Duan et al., 2016). In the test, the rotor was allowed to rotate freely under different wind speeds in order to better simulate the aerodynamic features of the wind turbine. A 1:40 model of OC3-Hywind Spar was carried out in the DHI Offshore Wave Basin in Hørsholm (Denmark). Comparisons were made between the experimental results and numerical analysis of FAST code (Tomasicchio et al., 2017).

Because the floater of the FOWT is in the water while the upper wind turbine is in the air, similar conditions of the Froude number and the Reynolds number should be met separately (De Ridder et al., 2014; Martin, 2011; Stewart et al., 2012; Jain et al., 2012). Hence, all the previous studies listed above used different techniques to mitigate such discrepancy. One solution proposed in the current study is to turn to the rule of thrust similarity.

The multiple megawatts Spar type FOWT is generally suitable for deep-sea areas with a water depth larger than 200 m. Meanwhile, for wind turbines located at the shallow

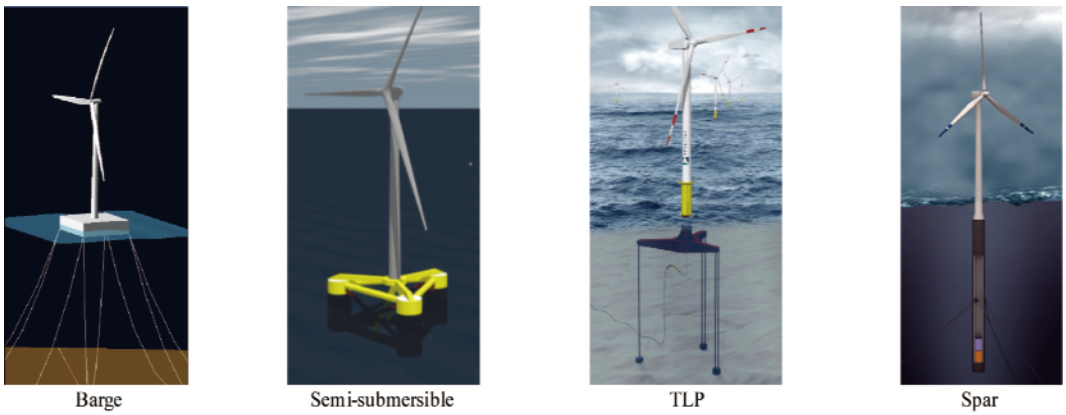

Fig. 1. Types of FOWT according to the principle of stability.

water area, bottom-fixed platform or other similar types of bases are enough to withstand the general environmental loadings. However, for a medium-depth water area with the water depth around 100 m, further discussion is necessary to propose a suitable Spar type FOWT solution, especially in considering the cost efficiency of the renewable energy. The concept of an optimal design as well as its coupled dynamic performance needs to be investigated in detail for future practical applications.

The present study proposes a 6MW Spar type FOWT with the designed water depth of 100 m. In order to obtain the aerodynamic performance of the rotor accurately, the thrust similarity model blades are used in the basin tests. Also, a 4×4 wind generation system is applied, which can generate different random wind sequences with higher precision.

The paper is studied by experimental and numerical methods, and the studies demonstrate that they are reliable for the designed 6MW Spar type FOWT. This paper is structured as follows. The 6MW Spar type FOWT system is described in Section 2. Section 3 introduces parameter settings of the numerical model. In Section 4, FOWT model and experimental set-up are described. Results and analysis are shown in Section 5, and the conclusion is drawn in Section 6.

2 6MW Spar type FOWT system

The 6MW Spar type FOWT system designed for water depth of 100 m includes four main components: a 3-blade wind turbine, a tower, a Spar type platform, and a catenary mooring system, as shown in Fig. 2. The arrow direction in Fig. 2 represents the positive direction of the motion of six degrees of motions. The draft of the Spar type platform is 76 m, and the hub height is 100 m. The essential parameters are briefly introduced in Table 1. Details of the wind turbine set-up could be referred to Meng et al. (2017a). Top diameter of the Spar type platform is designed as 8 m. The mooring system consists of three catenary cables. The right-handed coordinate system is applied in this study, the origin point is located at the mean water line, and *X*-axis is vertical to the wind rotor plane and parallel to the wind direction. From forward view to the positive *X*-axis, the direction of wind rotor rotation is clockwise. Compared with NREL (National Renewable Energy Laboratory) 5MW wind turbines, 6MW wind turbine has longer blade and thus harvests greater wind energy, which could be more cost effective.

3 Numerical model

The numerical model of a 6MW Spar type FOWT is constructed in the FAST v8.15. The FOWT model is subjected to the turbulent wind and irregular waves with blade pitch control strategy, which are all critical to the FOWT dynamic responses.

Turbulent wind generated by NREL TurbSim software (Jonkman and Kilcher, 2012) is adopted in the numerical

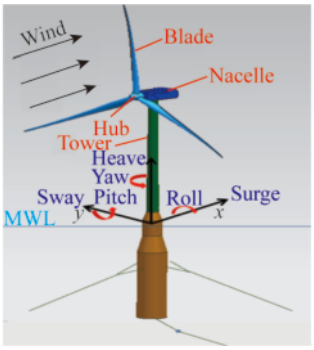

Fig. 2. Schematic of 6MW Spar type FOWT.

analysis. In the study of wind turbines, Kaimal wind spectrum is commonly used (Cai and Zhang, 2012). In this paper, it is applied with a vertical shear index of 0.14 and a surface roughness length of 0.03 m. The longitudinal power spectral density of Kaimal wind spectrum is shown in Eq. (1) (Moriarty et al., 2002).

$$S(f)=\frac{4\sigma^2 L/V_{\text{hub}}}{(1+6fL/V_{\text{hub}})^{5/3}}, \tag{1}$$

where f denotes the frequency, S represents the power spectral density, σ is the standard deviation of wind speed, L is the length parameter, and V_{hub} is the wind speed at the hub height.

Referred to the Karimirad and Moan (2012b), JONSWAP wave spectrum is applied and shown in Eq. (2).

$$S_\zeta(w)=319.34\frac{h_{1/3}^2}{T^4w^5}\exp\left(-\frac{1948}{T^4w^4}\right)3.3^{\exp\left[-\frac{(0.159wT-1)^2}{2\sigma^2}\right]} \tag{2}$$

where $h_{1/3}$ denotes the significant wave height, T represents the period, σ is the wave spectrum type parameter, and w is the wave frequency.

The control strategy of *PID* (Proportional Integral Differential) regulation of blade pitch is adopted and shown in Eq. (3).

$$u(t)=K_{\text{P}}e(t)+K_{\text{I}}\int_0^t e(t)\text{d}t+K_{\text{D}}\frac{\text{d}e(t)}{\text{d}t}, \tag{3}$$

where K_{P}, K_{I}, and K_{D} are the proportional coefficient, integral coefficient, and differential coefficient, respectively. $e(t)$ represents deviation signal, and $u(t)$ is the control volume.

After repeated calculation and verification, it is found that under the working conditions, the calculation result of 30 minutes simulation time tends to be stable. However, as the extreme sea state of the wind turbine motion is more intense, the results will be stabilized in about an hour. Simulations last 30 min and 1 hour for the working conditions and extreme sea state, respectively. Also, additional 30 seconds were applied before dynamic simulations to eliminate any start-up transient behavior. For more information about the effect of simulation time on Spar FOWT dynamic responses, see Meng et al. (2018).

Tsugane (2005) proposed using the momentum and en-

Table 1 6MW Spar type FOWT system performance parameters

Components	Item	Unit	Value	
			Prototype values	Model values
Wind turbine	Blade length	m	78	1.2
	Hub radius	m	2.35	0.036
	Cut-in wind speed	m/s	3	0.37
	Cut-out wind speed	m/s	25	3.09
	Rated wind speed	m/s	10.5	1.3
	Rated rotor speed	rpm	10	80.81
	Hub center height	m	100	1.53
Tower	Tower top diameter	m	4.8	0.07
	Tower top above waterline	m	96.8	1.48
	Tower bottom diameter	m	8	0.12
	Tower bottom above waterline	m	13	0.20
Spar type platform	Design water depth	m	100	1.53
	Design draft	m	76	1.16
	Platform length	m	89	1.36
	Platform COG (Center of Gravity) (including ballast)	m	−62.3	−0.95
	Platform COB (Center of Buoyancy)	m	−41.2	−0.63
	Diameter at waterline	m	9.5	0.15
	Drainage volume	m^3	11 421	0.04
	Moment of inertia (I_{xx})	$kg·m^2$	$2.5×10^9$	2.11
	Moment of inertia (I_{yy})	$kg·m^2$	$2.5×10^9$	2.11
	Moment of inertia (I_{zz})	$kg·m^2$	$2.5×10^8$	0.21
Mooring system	Number of the catenary	−	3	3
	Angle between catenary	°	120	120
	Total length of catenary	m	400	6.13
	Equivalent cross-sectional diameter	mm	130	1.99
	Weight per meter in water	N/m	3 495	0.8
	The horizontal distance between mooring point and platform center line	m	385.5	5.9
	Equivalent stiffness	kN	801 692.19	2.88
	Fairlead position	m	−21	−0.32

ergy conservation theory to solve the second-order average wave force by integrating on the far-field radiation surface. For a single frequency regular wave, the average wave force is:

$$\overline{F_t^{(2)}} = {\zeta_{\mathrm{a}j}}^2 T_{F_i}\left(\omega_j\right), \tag{4}$$

where $\zeta_{\mathrm{a}j}$ is the j-th incident wave amplitude, ω is the circular frequency and $T_{F_i}\left(\omega_j\right)$ is the quadratic transfer function.

Then the quadratic transfer function of the average wave force is:

$$T_{F_i}\left(\omega_j\right) = \overline{F_t^{(2)}}/{\zeta_{\mathrm{a}j}}^2. \tag{5}$$

For irregular waves, the second-order average wave force is:

$$\begin{aligned}\overline{F_t^{\mathrm{irr}}} &= \sum_{j=1}^{N} {\zeta_{\mathrm{a}j}}^2 T_{F_i}\left(\omega_j\right) = \sum_{j=1}^{N} 2S\left(\omega_j\right)\Delta\omega T_{F_i}\left(\omega_j\right) \\ &= 2\int_0^{\infty} T_{F_i}\left(\omega_j\right) S(\omega)\,\mathrm{d}\omega.\end{aligned} \tag{6}$$

Thus, the second-order average wave force of the irregular wave can be written as:

$$\overline{F_t^{\mathrm{irr}}} = 2\int_0^{\infty} \frac{\overline{F_t^{(2)}}}{{\zeta_{\mathrm{a}j}}^2} S(\omega)\,\mathrm{d}\omega, \tag{7}$$

where $\Delta\omega$ is the wave difference frequency and $S(\omega)$ is the wave spectral density function.

The typical motions of the moored floating structure include not only the first-order wave-frequency motion, but also the long-period second-order slow-drift motion. This is due to the small horizontal recovery force of the mooring system. Thus, low-frequency resonance motion is generated, which induces large mooring force and low-frequency slow drift motion. Formula for calculating second-order wave slow drift force spectrum based on quadratic transfer function and irregular wave spectrum is shown:

$$S_{F_t^{(2)}}(\mu) = 2\int_0^{\infty} S_\zeta(\omega) S_\zeta(\omega+\mu)\left|T_{jk}(\omega,\omega+\mu)\right|^2 \mathrm{d}\omega, \tag{8}$$

where, μ is the wave difference frequency and $\left|T_{jk}(\omega,\omega+\mu)\right|^2$ is the quadratic transfer function of the second-order force of difference frequency.

4 Experimental model and set-up

4.1 Scale methodology

In order to predict the aerodynamic characteristics of the prototype wind turbine accurately, geometrical similarity, kinematical similarity, dynamical similarity, and structural stiffness similarity are satisfied (Zhao et al., 2016a, 2016b).

The 1:65.3 scale ratio is applied in the present study.

A single-column wind turbine system is installed atop a flexible tower. Its flexibility has a great influence on the movement of the wind turbine system, such as the pitch motion response. Therefore, the model and prototype tower strictly follow the similar structural stiffness.

$$\frac{E_s I_s}{(EI)_m} = \lambda^5, \tag{9}$$

where, λ is the scale parameter, the subscript s refers to the prototype and m to the model, E is the Young's modulus of the tower structure, and I is the sectional moment of inertia. Conversion relationship between model and prototype is displayed in Table 2. For more information about the scale methodology, refer to Meng et al. (2017b).

4.2 Wind turbine model

In this paper, experimental lightweight blades are made of carbon fiber, as shown in Fig. 3. And the weight of the blades is strictly controlled. It should be noted that blades are redesigned in accordance with similar thrust. The NACA4412 airfoil which is suitable for a low Reynolds number (Hua et al., 2010) is used here.

The nacelle model is shown in Fig. 4 and Fig. 5. The key to the design of nacelle is to control the cabin weight. Material of aluminum alloy 2024 is adopted in the model nacelle.

Structural stiffness similarity and geometrical similarity in lengths are satisfied between model tower and prototype tower. The model tower has the inner diameter of 25 mm and its total length is divided into five sections. The length of 1.28 m is obtained according to the geometrical similarity as shown in Fig. 6.

4.3 Wind generation system

In the test, a new wind generation system is applied (Meng et al., 2017b). The device consists of 4×4 frequency-converting electric axial flow fans equipped with control devices to generate the wind field required for wind turbine model tests as shown in Fig. 7. The dimensions of the effective wind output area are 3 m×3 m. The wind generation system can generate random wind sequences required.

4.4 Wave generation system

The wave load is applied by the multi-unit wave generation system of Rexroth (Bosch Group) made in the Netherlands (Meng et al., 2017b). The sampling frequency of 40 Hz is selected in the test. The test time of each working condition is 30 minutes, which stands for more than three-hour

Table 2 Conversion relationship between model and prototype

Item	Symbol	Scale ratio	Item	Symbol	Scale ratio
Line scale	L_s/L_m	λ	Angular velocity	φ'_s/φ'_m	$\lambda^{-1/2}$
Line speed	V_s/V_m	$\lambda^{1/2}$	Period scale	T_s/T_m	$\lambda^{1/2}$
Line acceleration	a_s/a_m	1	Frequency scale	f_s/f_m	$\lambda^{-1/2}$
Angle scale	φ_s/φ_m	1	Wave force	F_s/F_m	$\gamma\lambda^3$
Area scale	A_s/A_m	λ^2	Wave moment	M_s/M_m	$\gamma\lambda^4$
Volume scale	∇_s/∇_m	λ^3	Thrust scale	F_s/F_m	λ^3
Water density	ρ_s/ρ_m	γ	Torque scale	M_s/M_m	λ^4
Quality (displacement)	Δ_s/Δ_m	$\gamma\lambda^3$	Power scale	P_s/P_m	$\lambda^{7/2}$

Fig. 3. Model blade based on the thrust similarity.

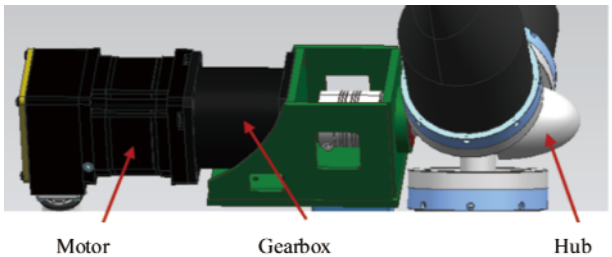

Fig. 4. Schematic diagram of nacelle model.

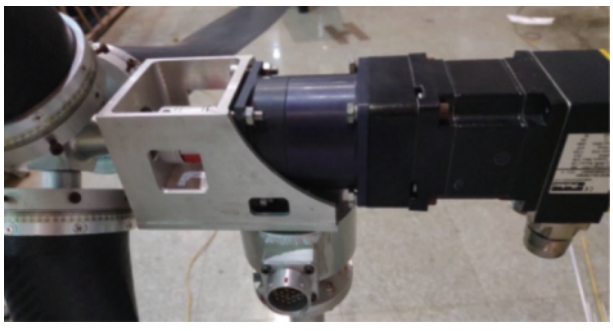

Fig. 5. Manufacturing production of nacelle model.

Fig. 6. Model tower with the length of 1.28 m.

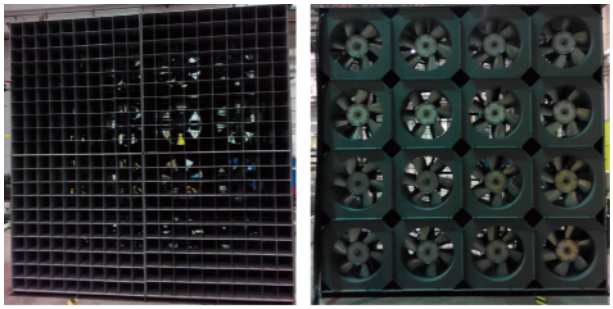

(a) Front (b) Rear

Fig. 7. Wind generation device with the form of 4×4 arrangement.

time length in reality. Note that data are collected after the test model reaches a stable motion state. Double plate multi-unit wave generation system is shown in Fig. 8.

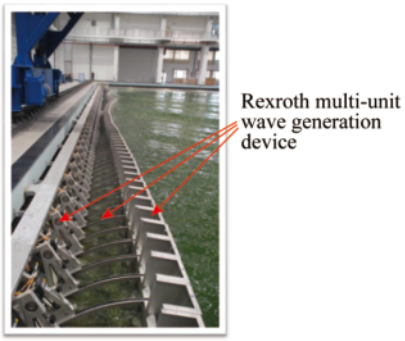

Fig. 8. Double plate multi-unit wave generation system (Meng et al., 2017b).

4.5 Test and measurement configuration

In the test, the wind speed measurement was carried out using a hot film wind speed transmitter, as shown in Fig. 9. The wind speed transmitter uses a new wind speed sensor that combines the advantages of high-quality film measurement technology and plastic packaging technology, which makes the wind speed sensitive component durable and has excellent anti-pollution capability. Thus, the wind speed measurement has accurate and reliable results as well as long-term stability.

The type of the torque speed sensor in the test is ZJ-0.5AM, as shown in Fig. 10a. The sensor not only measures the torque of the wind rotor, but also provides the rotation speed of the wind rotor. In the wind turbine test, by given a certain rotation speed of the wind rotor, the sensor can detect the actual value when operating. The TS-3000 torque speed power acquisition instrument is shown in Fig. 10b. The torque, speed and power can be displayed in real time.

The six-degree of freedom (DoF) force sensor is another important instrument, which is calibrated before experiment as shown in Fig. 11.

All the dimensions of model components are determined according to the model scale ratio, and the error does not exceed 1 mm. The weight of the model is less than the required weight and the ballast is used to meet the required weight distribution, including the total mass, center of gravity and radius of inertia. The error of the COG of the model is not more than 3%, and the pitch and roll inertia radius er-

Fig. 9. SERIES EE65 hot film wind speed transmitter.

(a) Torque sensor (b) TS-3000 torque speed power collector

Fig. 10. ZJ-0.5AM type torque measurement system.

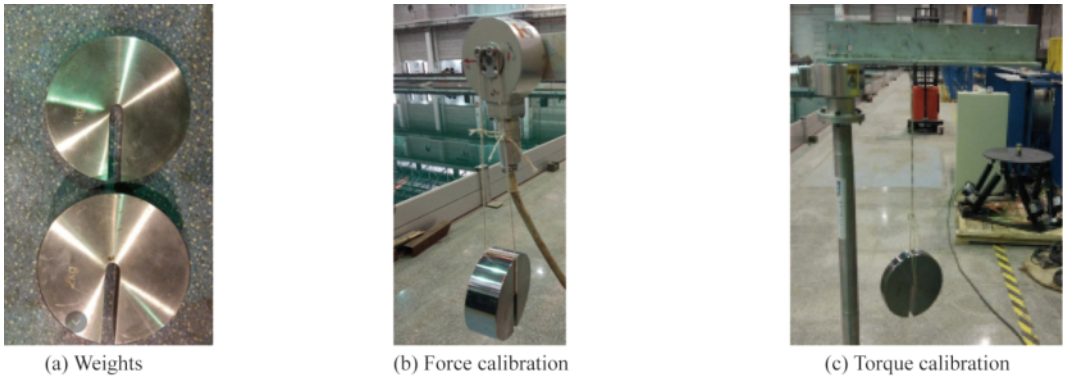

(a) Weights (b) Force calibration (c) Torque calibration

Fig. 11. Instrument calibration.

rors are not more than 5%.

4.6 Test conditions

In the still water test, the horizontal stiffness of the mooring system is tested. The model inertia was adjusted before the test, as shown in Fig. 12, and the detailed adjustment was done after the model floated in the basin.

Fig. 12. COG adjustment of 6MW Spar type FOWT model system.

In the wind-induced only test, three loading cases under different wind speeds were carried out, including the wind speed (Wind-1) below the rated one, the rated wind speed (Wind-2) and the cut-out wind speed (Wind-3). The specific parameters are shown in Table 3.

In the wave-induced only test, irregular waves of four different parameters were used in the test, as shown in Table 4, which contains irregular waves of a 50-year period. The spectral parameter γ in Table 4 is selected according to the ocean observation data which are detailedly described in Jonkman (2007) and Zhao et al. (2018).

The combined wind, wave and current tests were carried out, and the key performance parameters such as the aerodynamic performance of the wind turbine and the stress of the anchor chain were tested. Under the extreme sea conditions, the wind turbine stops operating, and the blade pitch angle is 90°. Therefore, the wind load is not applied in the combined wind, wave and current test condition LC4. And the specific parameters are shown in Table 5. The test graph is shown in Fig. 13.

5 Results and analysis

All the experimental and numerical results, including still water test, wind-induced only test, wave-induced only test and combined wind-wave-current test, are summarized. Note that these results have been converted to full scale by using Froude scaling.

5.1 Still water tests

In the still water test, initial displacements along the surge direction are enforced to the model mooring system, and the restoring forces under different initial displacements are obtained respectively, as shown in Fig. 14. It can be seen that the surge restoring force-displacement curve has a linear trend. The design of the model mooring system satisfies the test requirements. And the horizontal stiffness parameters of the anchor chain are obtained, which is beneficial to further modification of the numerical model.

In the still water test, the six DoFs motions are tested. By applying initial displacements to the test model, the decay curves of the surge, pitch and heave motion are obtained, which are very important motion forms of Spar FOWT, as shown in Fig. 15. The natural periods of the surge, pitch and heave motions are given in Table 6, which indicates that the experimental results have a good agree-

Table 3 Wind-induced only test conditions

Conditions	Mean wind speed (m/s)		Rotor speed (rpm)		Blade pitch (°)	Description
	Prototype	Model	Prototype	Model		
Wind-1	8	0.990	9.2	74.344	−3	Below rated wind speed
Wind-2	10.5	1.299	10	80.808	0	Rated wind speed
Wind-3	25	3.094	10	80.808	15	Cut-out wind speed

Table 4 Wave-induced only test conditions

Load cases	Significant wave height (m)		Peak period (s)		Spectral parameter γ	Description
	Prototype	Model	Prototype	Model		
Wave-1	2.5	0.038	9.8	1.213	1.0	Sea state corresponding to below rated wind speed
Wave-2	3	0.046	10.0	1.237	1.0	Sea state corresponding to rated wind speed
Wave-3	5.9	0.090	11.3	1.398	1.0	Sea state corresponding to cut-out rated wind speed
Wave-4	14.4	0.221	13.3	1.646	2.4	Sea state corresponding to wind speed of 50 years a period

Table 5 Combined wind, wave and current tests conditions

Load cases	Wind load	Wave load	Current velocity (m/s)		Inflow direction (°)	Description
			Prototype	Model		
LC1	Wind-1	Wave-1	0.6	0.074	0	Sea state corresponding to below rated wind speed
LC2	Wind-2	Wave-2	0.6	0.074	0	Sea state corresponding to rated wind speed
LC3	Wind-3	Wave-3	0.6	0.074	0	Sea state corresponding to cut-out rated wind speed
LC4	No wind	Wave-4	2.0	0.247	0	Sea state corresponding to wind speed of 50 years a period

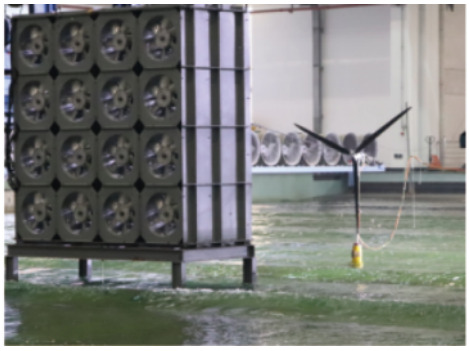

Fig. 13. Basin test of 6MW Spar type FOWT model system.

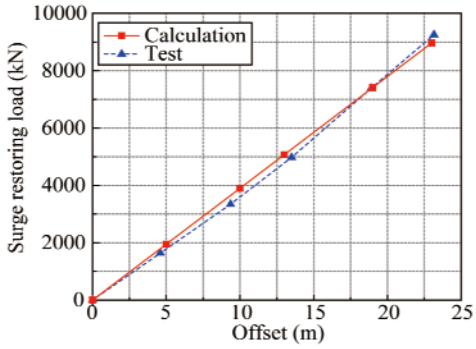

Fig. 14. Comparison of surge restoring loads between experimental and numerical results under different surge displacements.

ment with the numerical values. The natural periods are far away from the range of wave period, which may indicate a good motion performance in the wave.

5.2 Wind-induced tests

In the basin test, the redesigned wind turbine blade is installed, and the thrust force similarity between the model wind turbine and the prototype is satisfied. During the basin test, the speed of the rotor is controlled by the motor at the nacelle, and the pitch angle is manually adjusted. They both remain constant under each operating condition.

The uniformity of the wind speed and the turbulence intensity are presented in Fig. 16 (Meng et al., 2019). The wind speed surface represents the mean wind velocity time histories by smoothing. And the turbulence intensity surface is the corresponding temporal standard deviation of its time histories divided by the mean wind speed at each grid point. In the figure, the solid black circle defines the wind rotor plane in the wind field, and the black cross indicates the hub center. As observed from Fig. 16a, the wind speed basically spreads uniformly, except for some uneven part in the rotor plane. It is caused by the rotation effect of wind generators. Also, it can be seen in Fig. 16a, the high wind speed shows up near the bottom of the wind generation system, which can be explained by the wall effect. As the wind

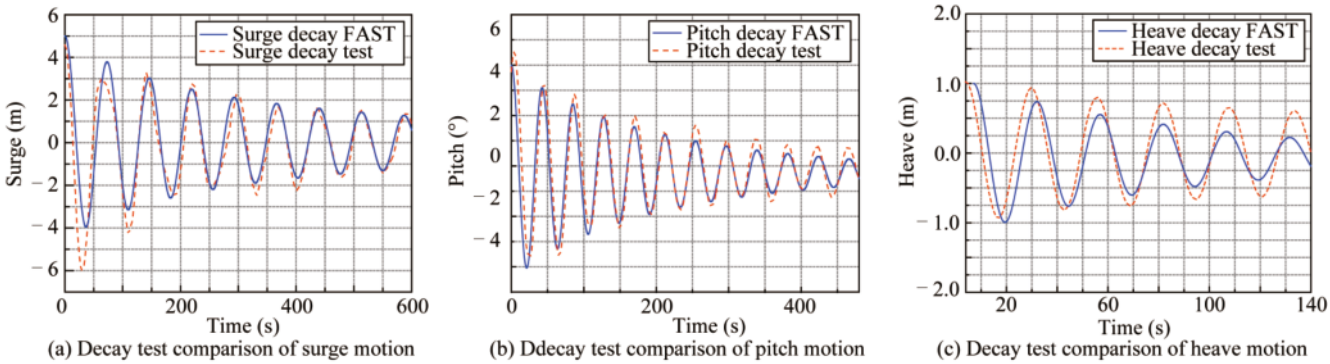

(a) Decay test comparison of surge motion between FAST and experimental results

(b) Ddecay test comparison of pitch motion between FAST and experimental results

(c) Decay test comparison of heave motion between FAST and experimental results

Fig. 15. Decay results comparison between experimental results and calculation values in still water.

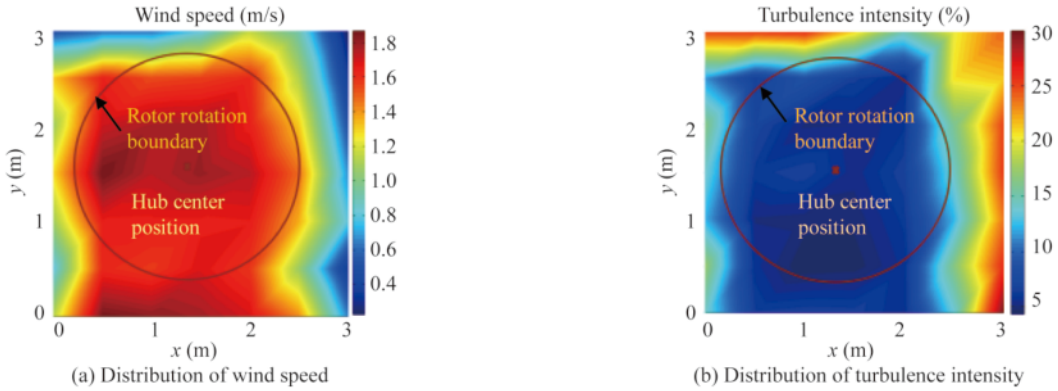

(a) Distribution of wind speed

(b) Distribution of turbulence intensity

Fig. 16. Distribution of wind speed and turbulence intensity.

Table 6 Still water decay results

Motions	Natural period T_d (s)	
	Test results	Calculation values
Surge	73.4	73.1
Pitch	41.1	42.4
Heave	25.9	25.1

generation system is placed directly on the ground, the wind speed at ground surface will be high. As to Fig. 16b, most areas of the rotor plane have the turbulence intensity smaller than 10%. Thus, the wind generation system applied in the present study is acceptable.

The comparison of the rotor thrust mean values between the experimental results and the numerical values is shown in Fig. 17. It can be seen from the figure that besides a good agreement, the maximum deviation of the rotor thrust is 9% at the cut-out wind speed under the numerical values. Under the cut wind speed, the wind speed is large, and the wind load on the blade surface is easy to separate. In the calculation and analysis, the air separation on the blade surface is not considered, and only some corrections are added. Thus, a large error of the calculated thrust occurred.

5.3 Wave-induced tests

The comparison between the measured wave spectrum and the target JONSWAP spectrum under the extreme sea conditions of 50 years is shown in Fig. 18. It can be seen that the irregular waves simulated in the deep-water basin test have high precision and meet the test requirements.

The statistical values of the surge, pitch and heave motions under the wave-induced loading only are shown in Fig. 19. It can be seen from figures that the surge, pitch and heave motion response as well as their standard deviation of the FOWT increase with the increasing severity of the wave load. The maximum response is obtained under the extreme sea state, which are 16.1 m, 9.3° and 1.8 m, respectively, for the surge, pitch and heave motion.

The overall trend of the numerical results is in good agreement with that of the experimental values, with some deviations. These deviations can be explained by the coupling motion between the cables from the rear of the nacelle and the FOWT slightly increased the experimental value (Fitzgerald, 2014).

5.4 Combined wind, wave, and current tests

Figs. 20−22 show the comparisons of Spar type platform surge, pitch and heave motion between test results and numerical values under combined wind−wave−current conditions. The trend of the platform motion characteristics seems consistent with the experimental value with respect to the trend characteristics, with the numerical value slightly smaller. Under the extreme sea state, the maximum response values of numerical results are 11.1%, 7.6%, and 13.5% smaller than the test results, respectively. One reas-

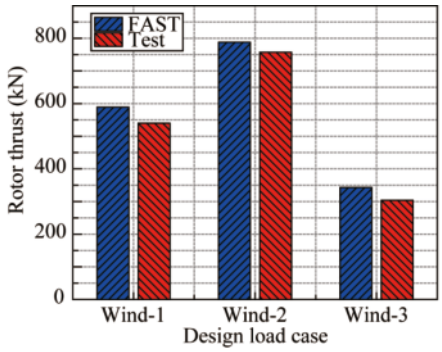

Fig. 17. Comparison of rotor thrust mean values between calculated and experimental results under wind-induced tests.

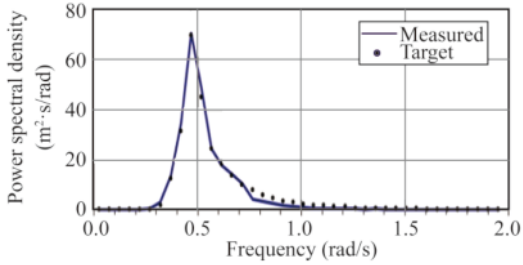

Fig. 18. Comparisons of wave spectrum between the target and measured results under extreme condition

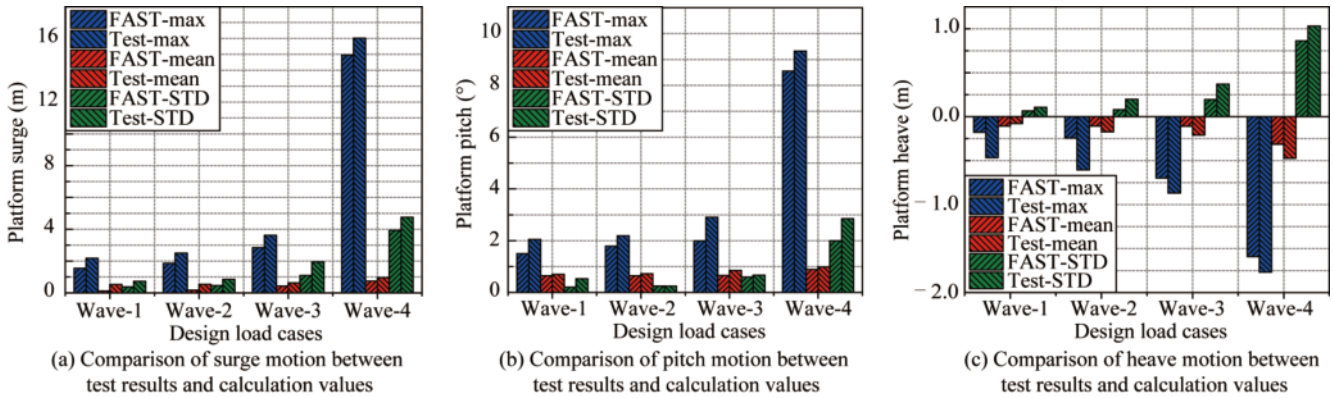

Fig. 19. Comparison of surge, pitch and heave motion between test results and calculation values under wave-induced only conditions.

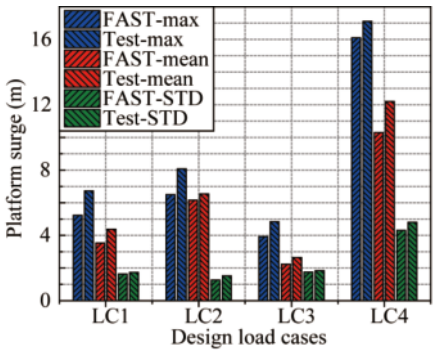

Fig. 20. Comparison of Spar type platform surge motion between test results and calculation values under combined wind, wave and current testing conditions.

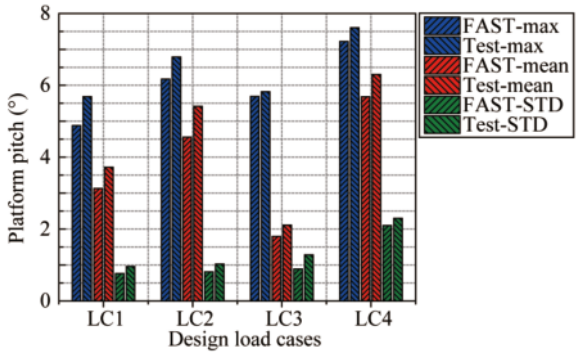

Fig. 21. Comparison of Spar type platform pitch motion between test results and calculation values under combined wind, wave and current testing conditions.

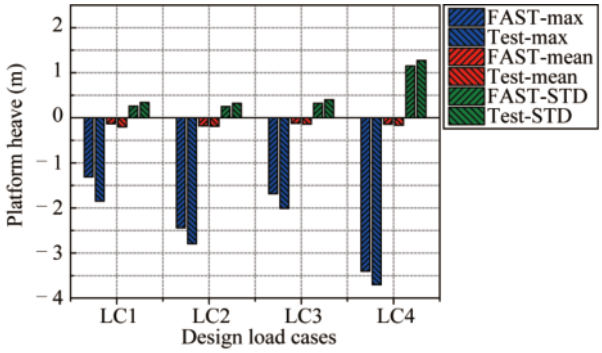

Fig. 22. Comparison of Spar type platform heave motion between test results and calculation values under combined wind, wave and current testing conditions.

on is that the environmental conditions in the numerical calculation have a certain deviation from the real metocean data. Another reason could be the scaling effect that is inevitable in model wave basin tests. Also, the influence of the swing motion of the cable from the rear of the nacelle on the FOWT is not considered in the calculation process. However, the Spar type FOWT numerical model established in FAST still has certain reliability and can be used for subsequent numerical studies.

It can be seen from Fig. 20 that compared with the wave-induced only tests, the maximum test response result of the platform surge motion is increased by 6.7% under the extreme sea conditions. Since the wind turbine stops, it is not affected by the wind load, which indicates that the addition of the current loading amplifies the surge motion and increases the offset of the FOWT at the equilibrium position in the horizontal plane.

Fig. 21 shows the comparison between the numerical value of the pitch motion response and the experimental value under the combined wind-wave-current conditions. It can be seen that the maximum value and the mean value of the platform pitch motion are the largest at the rated wind speed. This is because the wind turbine thrust reaches the maximum value, which indicates that the platform pitch motion response is greatly affected by the wind load. Under extreme sea conditions, the platform pitch motion has a value of 7.6°. According to the criteria for FOWT design, the Spar type FOWT should have a pitch angle smaller than 10° (Det Norske Veritas, 2016). Thus, the design of 6MW Spar type FOWT meets the specifications. In addition, as the working conditions get more severe, the standard deviation of the platform pitch increases. This shows that the pitch motion fluctuation of the platform is affected by the wave and current loads.

Fig. 22 shows the comparison between the numerical values of the heave motion response and the experimental values under the combined wind-wave-current testing conditions. It can be seen from the figure that compared with the wave-induced only tests, the platform heave motion response is significantly increased under the combined effect of wind, wave and current. Under the extreme sea conditions, the maximum value of the heave motion is −1.77 m under wave-induced only condition. When the current loading is added, it turns to be −3.7 m. Thus, the addition of the current load increases the maximum value of the platform heave motion.

5.5 Frequency analysis

In the present section, the spectral analysis was contracted to reveal the dynamic characteristics of the 6MW Spar type FOWT. Four wave-included only test conditions and combined wind-wave-current test conditions were analyzed in frequency domain, but for simplicity, only the wave-3 test condition and LC3 test condition were selected to illustrate the observed coupled dynamic response of surge, pitch and heave. Fig. 23 shows the comparisons of the motion spectra between the model tests and the numerical simulations for wave-3 test condition and LC3 test condition. The spectra results obtained from numerical simulation show good agreement with that of model test.

It is found that the surge spectra peak occurs approximately at surge nature frequency, which suggests that the resonance response at this frequency is a consequence of the platform being excited by the incident waves near its natur-

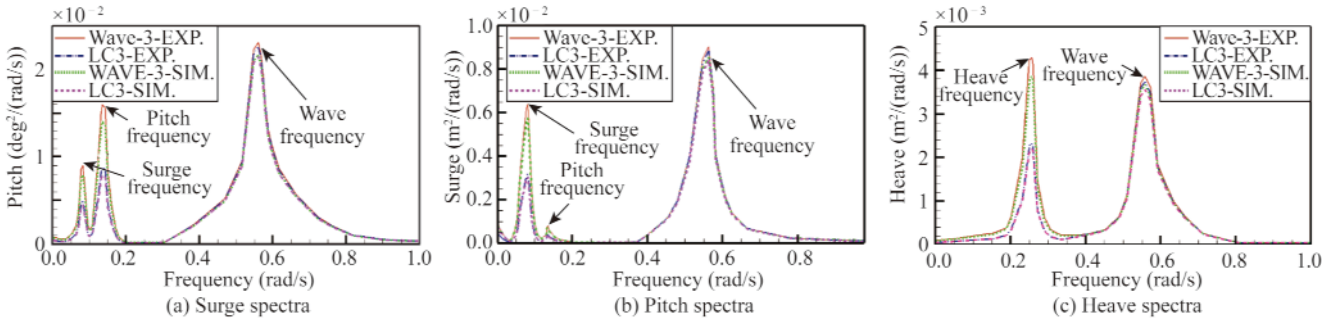

Fig. 23. Comparisons of motion spectra between the model tests and wave-3 test condition and LC3 test condition.

al frequency as shown in Fig. 23a. For the same reason, the resonance responses of the pitch and heave at the respective nature frequency are also controlled by the natural frequency as shown in Figs. 23b and 23c. In addition, it is found that the surge and pitch motions are strongly coupled with one another. However, the heave response is significantly different from surge and pitch response behavior, which shows that the heave motion is not subject to any coupling effects and independent from the surge and pitch. Furthermore, through the comparison of wave-3 only test conditions and the combined wind−wave−current test conditions, it is found that the wind and current forces neither significantly shift the peak frequencies nor change the peak amplitudes at wave frequencies, but the peak value at lower frequency (the natural frequency) is substantially reduced possibly due to the oscillation-decreasing characteristic of the wind and current loads on the low frequency response. It means that the wind and current forces can decrease the low frequency oscillation, which benefits the fatigue maintenance of the mooring system.

6 Conclusions

In this paper, the comprehensive experimental set-up was established and improved, which can simulate the wind, wave and current loads accurately. The wind, wave and current loads used in the model test have high precision. The numerical calculation and experimental research methods are both used to study the dynamic responses of the 6MW Spar type FOWT. The results show that:

(1) In the still water test, the mooring stiffness curves of the delta-line mooring system and the 6-DoFs natural periods of the 6MW Spar type FOWT are obtained. The theoretical calculations agree well with the experimental values.

(2) Under the condition of wind-induced only tests, the rotor thrust reaches the maximum value under the rated wind speed condition. Compared with the test value, the maximum deviation of the numerical value is 9%, which agrees well with the experimental values.

(3) Under the condition of wave-induced only tests, the platform surge, pitch and heave motion responses increase with the increasing wave load, and the maximum response is achieved under the extreme sea conditions. The maximum value of the surge motion is 16.1 m. The maximum pitch angle is 9.3°, and the maximum response of the heave is 1.77 m.

(4) Under the combined wind, wave and current tests conditions, the comparisons between the numerical values and the experimental values of the platform surge, pitch and heave motion performances are carried out. The results show that under the extreme sea state, the addition of the current load increases the surge motion, reduces the extreme value of platform pitch motion response, and aggravates the fluctuation of the heave motion.

(5) Through the spectra analysis, it is found that the wind and current loads can decrease the low frequency oscillation of the FOWT system.

A combination of model basin test method and numerical analysis method is applied in the paper. The research proves that the 6MW Spar type FOWT concept used in this paper has a better motion performance. The research can also provide some guidance for further development of FOWT.

In the future basin tests, in order to reduce the deviation between the test results and the calculated value, the method of reducing the weight of the motor and the cable of the motor at the nacelle will be applied. Under the extreme sea conditions, the calculation method of the motion responses under accidental conditions such as the failure of an anchor chain needs to be further investigated. In addition, in order to further investigate the effect of the second order wave force on the motion of the FOWT system, a detailed analysis will be carried out in our future research.

References

Cai, J.F. and Zhang, Y., 2012. Differences of Kaimal and von Karman turbulence spectrum model in wind turbine load calculation, *Wind Energy*, (3), 80–84. (in Chinese)

Cermelli, C., Roddier, D. and Aubault, A., 2009. WindFloat: a floating foundation for offshore wind turbines-Part II: Hydrodynamics analysis, *Proceedings of ASME 2009 28th International Conference on Ocean, Offshore and Arctic Engineering*, Honolulu, Hawaii, USA.

Chaviaropoulos, P.K. and Hansen, M.O.L., 2000. Investigating three-dimensional and rotational effects on wind turbine blades by means of a quasi-3D Navier-Stokes solver, *Journal of Fluids Engineering*,

122(2), 330–336.

Contestabile, P., Ferrante, V. and Vicinanza, D., 2015. Wave energy resource along the coast of Santa Catarina (Brazil), *Energies*, 8(12), 14219–14243.

De Ridder, E.J., Otto, W., Zondervan, G.J., Huijs, F. and Vaz, G., 2014. Development of a scaled-down floating wind turbine for offshore basin testing, *Proceedings of ASME 2014 33rd International Conference on Ocean, Offshore and Arctic Engineering*, San Francisco, California, USA.

Det Norske Veritas (DNV), 2016. *Support Structures for Wind Turbines*, DNVGL-ST-0126, Standard Offshore, Det Norske Veritas, Oslo, Norway.

Duan, F., Hu, Z.Q. and Niedzwecki, J.M., 2016. Model test investigation of a spar floating wind turbine, *Marine Structures*, 49, 76–96.

Global Wind Statistics 2016, GWEC. http://www.gwec.net/.

Hua, X., Gu, R., Jin, J.F., Liu, Y.R., Ma, Y., Cong, Q. and Zhang, Y., 2010. Numerical simulation and aerodynamic performance comparison between seagull aerofoil and NACA 4412 aerofoil under low-Reynolds, *Advances in Natural Science*, 3(2), 244–250.

Iuppa, C., Cavallaro, L., Foti, E. and Vicinanza, D., 2015. Potential wave energy production by different wave energy converters around Sicily, *Journal of Renewable and Sustainable Energy*, 7(6), 061701.

Jain, A., Goupee, A.J., Robertson, A.N., Kimball, R.W., Jonkman, J.M. and Swift, A.H.P., 2012. FAST code verification of scaling laws for DeepCwind floating wind system, *Proceedings of 22nd International Offshore and Polar Engineering Conference*, Rhodes, Greece.

Jeon, M., Lee, S. and Lee, S., 2014. Unsteady aerodynamics of offshore floating wind turbines in platform pitching motion using vortex lattice method, *Renewable Energy*, 65, 207–212.

Jonkman, J.M., 2007. *Dynamics Modeling and Loads Analysis of an Offshore Floating Wind Turbine*, National Renewable Energy Laboratory, USA.

Jonkman, J., 2010. *Definition of the Floating System for Phase IV of OC3*, National Renewable Energy Laboratory, USA.

Jonkman, J.M. and Kilcher, L., 2012. *TurbSim User's Guide*, Version 1.06.00, National Renewable Energy Laboratory, USA.

Karimirad, M., 2011. *Stochastic Dynamic Response Analysis of Spar-Type Wind Turbines with Catenary or Taut Mooring Systems*, Ph.D. Thesis, Norwegian University of Science and Technology, Trondheim.

Karimirad, M. and Moan, T., 2012a. A simplified method for coupled analysis of floating offshore wind turbines, *Marine Structures*, 27(1), 45–63.

Karimirad, M. and Moan, T., 2012b. Wave- and wind-induced dynamic response of a Spar-type offshore wind turbine, *Journal of Waterway*, *Port*, *Coastal*, *and Ocean Engineering*, 138(1), 9–20.

Kvittema, M.I., Bachynski, E.E. and Moan, T., 2012. Effects of hydrodynamic modelling in fully coupled simulations of a semi-submersible wind turbine, *Energy Procedia*, 24, 351–362.

Marino, E., Giusti, A. and Manuel, L., 2017. Offshore wind turbine fatigue loads: The influence of alternative wave modeling for different turbulent and mean winds, *Renewable Energy*, 102, 157–169.

Martin, H.R., 2011. *Development of a Scale Model Wind Turbine for Testing of Offshore Floating Wind Turbine Systems*, MSc. Thesis, The University of Maine, Orono, ME.

Matha, D., 2010. *Model Development and Loads Analysis of an Offshore Wind Turbine on a Tension Leg Platform with a Comparison to Other Floating Turbine Concepts*, National Renewable Energy Laboratory, USA.

Meng, L., He, Y.P., Liu, Y.D., Zhao, Y.S., Tong, J. and Yu, L., 2018. Numerical study on influence of turbulent and steady winds on coupled dynamic response of 6-MW Spar-type FOWT, *Proceedings of the 28th International Ocean and Polar Engineering Conference*, Sapporo, Japan.

Meng, L., He, Y.P., Zhao, Y.S., Peng, T. and Kou Y.F., 2017b. Research and practice of offshore wind turbine model test platform and technology, *Scientia Sinica Physica*, *Mechanica and Astronomica*, 47(10), 104701.

Meng, L., He, Y.P., Zhao, Y.S., Peng, T. and Yang, J., 2019. Experimental study on aerodynamic characteristics of the model wind rotor system and on characterization of a wind generation system, *China Ocean Engineering*, 33(2), 137–147.

Meng, L., Zhou, T., He, Y.P., Zhao, Y.S. and Liu, Y.D., 2017a. Concept design and coupled dynamic response analysis on 6-MW Spar-type floating offshore wind turbine, *China Ocean Engineering*, 31(5), 567–577.

Moriarty, P.J., Holley, W.E. and Butterfield, S., 2002. Effect of turbulence variation on extreme loads prediction for wind turbines, *Journal of Solar Energy Engineering*, 124(4), 387–395.

Namik, H. and Stol, K., 2010. Individual blade pitch control of floating offshore wind turbines, *Wind Energy*, 13(1), 74–85.

Nejad, A.R., Bachynski, E.E., Kvittem, M.I., Luan, C.Y., Gao, Z. and Moan, T., 2015. Stochastic dynamic load effect and fatigue damage analysis of drivetrains in land-based and TLP. Spar and semi-submersible floating wind turbines, *Marine Structures*, 42, 137–153.

Nielsen, F.G., Hanson, T.D. and Skaare, B., 2006. Integrated dynamic analysis of floating offshore wind turbines, *Proceedings of the 25th International Conference on Offshore Mechanics and Arctic Engineering*, Hamburg, Germany.

Quallen, S., Xing, T., Carrica, P., Li, Y.W. and Xu, J., 2013. CFD simulation of a floating offshore wind turbine system using a quasi-static crowfoot mooring-line model, *Proceedings of the 23rd International Offshore and Polar Engineering Conference*, Anchorage, Alaska.

Sahu, B.K., 2018. Wind energy developments and policies in China: A short review, *Renewable and Sustainable Energy Reviews*, 81, 1393–1405.

Salehyar, S. and Zhu, Q., 2015. Aerodynamic dissipation effects on the rotating blades of floating wind turbines, *Renewable Energy*, 78, 119–127.

Skaare, B., 2017. Development of the Hywind concept, *Proceedings of ASME 36th International Conference on Ocean, Offshore and Arctic Engineering*, Trondheim, Norway.

Skaare, B., Hanson, T.D., Nielsen, F.G., Yttervik, R., Hansen, A.M., Thomsen, K. and Larsen, T.J., 2007. Integrated dynamic analysis of floating offshore wind turbines, *Proceedings of the European Wind Energy Conference and Exhibition* (*EWEC*), Milan, Italy.

Soukissian, T., Karathanasi, F. and Axaopoulos, P., 2017. Satellite-based offshore wind resource assessment in the mediterranean sea, *IEEE Journal of Oceanic Engineering*, 42(1), 73–86.

Stewart, G.M., Lackner, M.A., Robertson, A., Jonkman, J. and Goupee, A.J., 2012. Calibration and validation of a FAST floating wind turbine model of the deepCwind scaled tension-leg platform, *Proceedings of the 22nd International Offshore and Polar Engineering Conference*, Rhodes, Greece.

Tomasicchio, G.R., Avossa, A.M., Riefolo, L., Ricciardelli, F., Musci, E., D'Alessandro, F. and Vicinanza, D., 2017. Dynamic modelling of a Spar buoy wind turbine, *Proceedings of the 36th International Conference on Ocean, Offshore and Arctic Engineering*, Trondheim,

Norway.

Tomasicchio, G.R., D'Alessandro, F., Avossa, A.M., Riefolo, L., Musci, E., Ricciardelli, F. and Vicinanza, D., 2018. Experimental modelling of the dynamic behaviour of a Spar buoy wind turbine, *Renewable Energy*, 127, 412–432.

Tran, T.T. and Kim, D.H., 2015. The aerodynamic interference effects of a floating offshore wind turbine experiencing platform pitching and yawing motions, *Journal of Mechanical Science and Technology*, 29(2), 549–561.

Tsugane, M., 2005. A study on ship's drifting in wind and wave, *The Journal of Japan Institute of Navigation*, 112, 133–140. (in Japanese)

Uihlein, A. and Magagna, D., 2016. Wave and tidal current energy - A review of the current state of research beyond technology, *Renewable and Sustainable Energy Reviews*, 58, 1070–1081.

Utsunomiya, T., Nishida, E. and Sato, I., 2009. Wave response experiment on Spar-type floating bodies for offshore wind turbine, *Proceedings of the 19th International Offshore and Polar Engineering Conference*, Osaka, Japan.

Wang, L. and Sweetman, B., 2013. Multibody dynamics of floating wind turbines with large-amplitude motion, *Applied Ocean Research*, 43, 1–10.

Wen, B.R., Dong, X.J., Tian, X.L., Peng, Z.K., Zhang, W.M. and Wei, K.X., 2018. The power performance of an offshore floating wind turbine in platform pitching motion, *Energy*, 154, 508–521.

Zhao, Y.S., She, X.H., He, Y.P., Yang, J.M., Peng, T. and Kou, Y.F., 2018. Experimental study on new multi-column tension-leg-type floating wind turbine, *China Ocean Engineering*, 32(2), 123–131.

Zhao, Y.S., Yang, J.M., He, Y.P. and Gu, M.T., 2016a. Dynamic response analysis of a multi-column tension-leg-type floating wind turbine under combined wind and wave loading, *Journal of Shanghai Jiaotong University* (*Science*), 21(1), 103–111.

Zhao, Y.S., Yang, J.M., He, Y.P. and Gu, M.T., 2016b. Coupled dynamic response analysis of a multi-column tension-leg-type floating wind turbine, *China Ocean Engineering*, 30(4), 505–520.